

# Microstructure and Solid/Liquid Interface Evolutions of Directionally Solidified Fe-Al-Ta Eutectic Alloy

CUI Chunjuan<sup>1,2</sup>, WANG Songyuan<sup>1</sup>, YANG Meng<sup>1</sup>, SU Haijun<sup>1</sup>, WEN Yagang<sup>1</sup>,  
WANG Pei<sup>1</sup>, REN Chiqiang<sup>1</sup>

(1. School of Metallurgical Engineering, Xi'an University of Architecture and Technology, Xi'an 710055, China; 2. Shaanxi Engineering Technology Research Center for Wear-resisting Materials, Xi'an 710055, China)

**Abstract:** A modified Bridgman directional solidification technique was used to prepare Fe-Al-Ta eutectic *in situ* composites at different growth rates ranging from 6 to 80  $\mu\text{m/s}$ . The directionally solidified Fe-Al-Ta eutectic composites are composed of two phases: Fe(Al,Ta) matrix phase, and Fe<sub>2</sub>Ta(Al) Laves phase. Solidification microstructure is affected by solidification rate. Microstructure of the Fe-Al-Ta eutectic alloy grown at 6.0  $\mu\text{m/s}$  is broken-lamellar eutectic. Eutectic colonies are formed with the increase of the solidification rate. Microstructures are mainly composed of the lamellar or fibrous eutectic at the center of the colony and coarse lamellar eutectic zone at the boundary. Meanwhile, the inter-lamellar spacing (or the inter-rod spacing) is decreased. The spacing adjustments are also observed in Fe-Al-Ta eutectic alloy. The solid/liquid interface evolves from planar interface to shallow cellular interface, then to deep cellular, and finally to shallow cellular planar with the increase of the solidification rate.

**Key words:** directional solidification; solidification rate; eutectic alloy; solid/liquid interface

## 1 Introduction

Intermetallic compound is a solid-state compound which exhibits metallic bonding, without defined stoichiometry and a long-range-ordered crystal structure. Due to the high creep resistance and tensile strength, this kind of material is widely used in the aeronautic, aerospace and high thrust-weight ratio engine industry<sup>[1-3]</sup>. Fe-Al intermetallic compound has been paid more attentions, because it has many characteristics, *e.g.*, low price, low density (6.5-7.2  $\text{g/cm}^3$ ), excellent anti-shake performance, superior oxidation resistance<sup>[4]</sup> and good corrosion resistance<sup>[5]</sup>, *etc.* However, the engineering application of the Fe-Al intermetallic

has been limited by its poor ductility at ambient temperature. In addition, its strength and creep resistance decrease above 600  $^{\circ}\text{C}$ <sup>[6]</sup>. In order to overcome these shortcomings, many investigations have been carried out, for example, mechanical alloying<sup>[7]</sup>, micro alloying by adding other trace elements, *e.g.*, Zr, Nb and Cr<sup>[8,9]</sup>, compounding by adding some continuous or discontinuous reinforced phases<sup>[10]</sup>, heat treatment<sup>[11]</sup>, and so on. Directional solidification technique is an attractive method to obtain well aligned microstructure by controlling crystal growth orientation along with the heat flow direction. This method can produce a significant strengthening effect on the material's mechanical properties, because the horizontal grain boundary is eliminated during solidification process<sup>[12]</sup>. Therefore, some refractory metals have been added into Fe-Al alloy to obtain eutectic composites by directional solidification technique<sup>[13-16]</sup>. In the present study Fe-Al-Ta eutectic *in situ* composites were prepared by a modified Bridgman directional solidification technique (which has a higher temperature gradient 150  $\text{K/cm}$ ) at the solidification rate of 6, 20, 30 and 80  $\mu\text{m/s}$ . Microstructure characteristics at different solidification rates were systematically studied and the mechanism of lamellar-rod eutectic transitions were also investigated. Moreover, morphologies of the solid/liquid interface at different

© Wuhan University of Technology and Springer-Verlag GmbH Germany, Part of Springer Nature 2019

(Received: May 18, 2018; Accepted: Feb. 21, 2019)

CUI Chunjuan (崔春娟): Ph D; Prof.; E-mail: cuichunjuan@xauat.edu.cn

Funded by the National Natural Science Foundation of China(No.51201121), 2015 Science and Technology Foundation for Selected Overseas Chinese Scholars of Shaanxi Province, Key Industry Innovation Chain (group) Project of Shaanxi Province (No.2019ZDLGY 04-04) International Science and Technology Cooperation and Exchange Program of Shaanxi Province (No.2016KW-055), Research Project of Shaanxi Engineering Technology Research Center for Wear-resisting Materials (No.2016NMZX03)

solidification rates were studied as well.

## 2 Experimental

99.9% pure iron, 99.999% pure aluminium and 99.95% Ta were mixed together and homogeneously melted to prepare the Fe85/Ta7/Al8 eutectic alloy ingots in vacuum ( $1.0 \times 10^{-2}$  Pa) using vacuum induction melting technique. The master alloy was obtained by cutting the middle of the ingot into  $\Phi 6 \times 100$  mm cylindrical bars. The alloy bars were put into a  $\text{Al}_2\text{O}_3$  crucible. The directional solidification experiments were carried out in a modified vertical Bridgman furnace at the solidification rate of 6, 20, 30 and 80  $\mu\text{m/s}$ . The cylindrical bars were melted locally by resistance heating under high purity Argon. As the crucible was slowly lowered into the region cooled by Ga-In-Sn liquid metal, a Fe-Al-Ta eutectic reaction took place, leading to the formation of the eutectic alloy. In order to obtain the morphology of solid/liquid interface, ingots were withdrawn into the cooling liquid (Ga-In-Sn alloy) for quenching when the growth length extended to about 90 mm.

The samples were wet ground and thereafter mechanically polished down with 3, 1, and 1/4  $\mu\text{m}$  diamond paste. Finally the specimen was etched in a solution of glycerine (68 vol%), 70%  $\text{HNO}_3$  (16 vol%) and 40% HF (16 vol%). The microstructure of the specimen was investigated by a scanning electronic microscope (SEM, JSM-5600LV) and an energy dispersive spectroscopy (EDS, JED2200) was used to investigate the phase composition. The solid/liquid interface morphologies were studied by optical microscope (OM, OHXMC50).

## 3 Results and discussion

### 3.1 Microstructure of the as-cast alloy and directionally solidified Fe-Al-Ta eutectic alloy

Microstructures of the as-cast alloy and typical directionally solidified Fe-Al-Ta eutectic on the longitudinal section are shown in Fig.1. The light phase is  $\text{Fe}_2\text{Ta}$  (Al) Laves phase, and the dark phase is Fe (Al, Ta) matrix phase. In Fig.1 (a), the coarse  $\text{Fe}_2\text{Ta}$  (Al) Laves phase can be clearly observed, and the eutectic structure grows as disordered colony. This is caused by the isotropic heat. Fig.1(b) shows the microstructure of directionally solidified alloy on the longitudinal section at the solidification rate of 20  $\mu\text{m/s}$ . It can be seen that the microstructure is directionally aligned and uniformly distributed owing to the directional heat flow. More-

over, the microstructure in Fig.1(b) is much more finer than that of Fig.1(a). This is caused by the higher cooling rate. It can also be seen from Fig.1(b) that the fibers are parallel to each other within the same grain but some fibers are deviated from the original direction at the grain boundaries. A grain boundary usually consists of structural units which depend on both the misorientation of the two grains and the plane of the interface. The types of structural unit that exist can be related to the concept of the coincidence site lattice, in which repeated units are formed from points where the two misoriented lattices happen to coincide. Moreover, dendrites are not found in directionally solidified Fe-Al-Ta eutectic alloy. The perfect microstructure of Fig.1(b) is caused by single heat flow and high temperature gradient of the modified Bridgman directional solidification technique (150 K/cm). Consequently, mechanic properties of the material can be improved as expected.

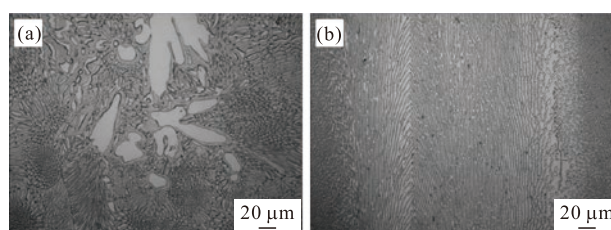


Fig.1 Longitudinal microstructures of the Fe-Al-Ta alloys: (a) master alloy; (b) directionally solidified eutectic alloy

### 3.2 Phase composition

Fig.2(a) and 2(b) are the energy dispersive spectrometer (EDS) patterns for the light phase and dark phase of the directionally solidified Fe-Al-Ta eutectic composite, respectively. The results show that the relationship between Fe atom and Ta atom is close to 2:1 in the light phase. That phase should be  $\text{Fe}_2\text{Ta}$  (Al) Laves phase. Moreover, in the dark phase, Fe is the major element, and small amount of Al and Ta are contained. This demonstrates that the dark phase is Fe (Al, Ta) matrix.

### 3.3 Effects of solidification rate on microstructure of directionally solidified Fe-Al-Ta eutectic alloy

#### 3.3.1 The mechanism of lamellar-rod eutectic transition

The solidification rate has a significant impact on the solidified microstructure. The transverse and longitudinal microstructures of Fe-Al-Ta eutectic at different solidification rates are shown in Fig.3, Fig.4, Fig.5 and Fig.6, respectively.

At the low solidification rate (6  $\mu\text{m/s}$ ), microstructure of the Fe-Al-Ta eutectic is regular broken-lamella eutectic structures as shown in Fig.3(a),

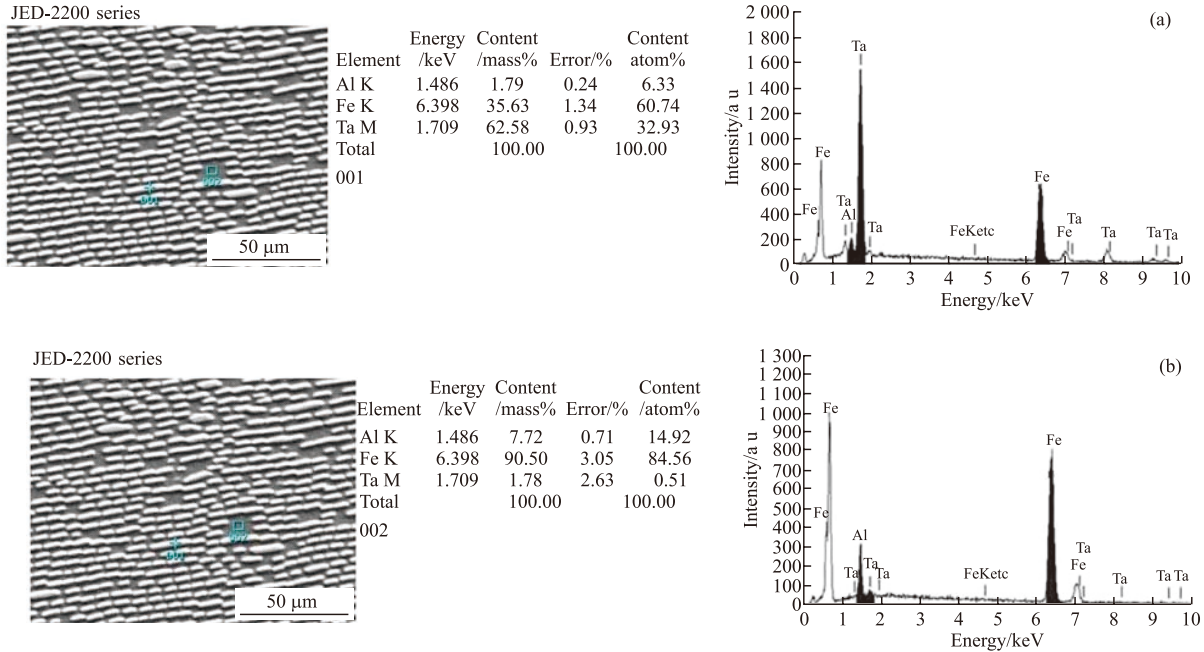


Fig.2 EDS patterns of the Fe-Al-Ta eutectic alloy prepared by Bridgman technique at the solidification rate of 6 μm/s: (a) the light phase; (b) the dark phase

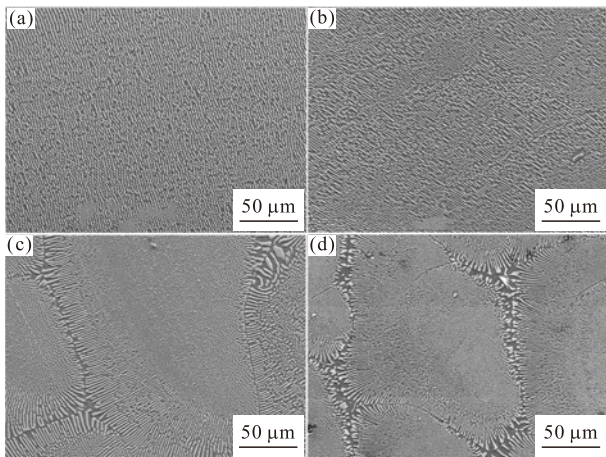


Fig.3 Steady transverse microstructures of directionally solidified Fe-Al-Ta eutectic alloy grown at (a)  $R=6 \mu\text{m/s}$ ; (b)  $R=20 \mu\text{m/s}$ ; (c)  $R=30 \mu\text{m/s}$ ; (d)  $R=80 \mu\text{m/s}$

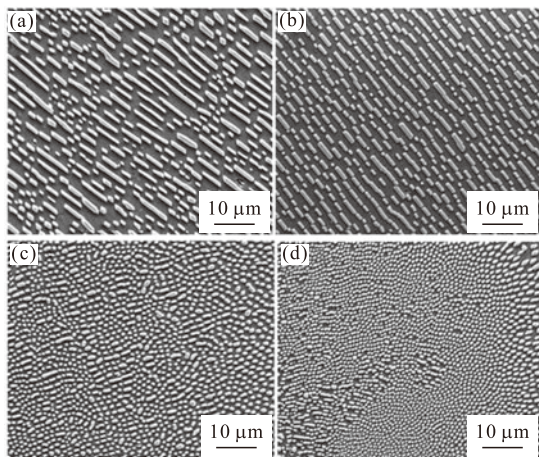


Fig.4 Steady transverse microstructures (greater magnification) of directionally solidified Fe-Al-Ta eutectic alloy grown at (a)  $R=6 \mu\text{m/s}$ ; (b)  $R=20 \mu\text{m/s}$ ; (c)  $R=30 \mu\text{m/s}$ ; (d)  $R=80 \mu\text{m/s}$

Fig.4(a), Fig.5(a) and Fig.6(a). With the increase of the solidification rate, eutectic colonies are formed and morphology of the Laves phase transforms from broken-lamella structure to rod-like structure as shown in Fig.4(b)-Fig.6(d). The fibers are parallel to each other within the same grain but some fibers are deviated from the original direction at the grain boundaries. The study of Tiller<sup>[17]</sup> showed that microstructure of the eutectic is determined by the crystal growth rate. Lower growth rate is beneficial to form lamellar eutectic structure, and higher growth rate is beneficial to form rod eutectic structure.

Liu *et al*<sup>[18]</sup> studied the dynamic effects in the lamellar-rod eutectic transition, the lamellar spacing was calculated to change to a larger rod spacing to achieve lower undercooling. Some lamellae would transform to rods in the region, which satisfies the following relationship:

$$\Delta T_{Rm} < \Delta T_{LM} < \Delta T_{RM} \tag{1}$$

where  $\Delta T_{Rm}$  is the minimum rod undercooling,  $\Delta T_{RM}$  is the maximum rod undercooling, and  $\Delta T_{LM}$  is the maximum lamellar undercooling, respectively. For Fe-Al-Ta alloy, the lamellar-rod transition may result from higher undercooling. Generally speaking, the increase of the solidification rate would result in large constitutional undercooling, the higher undercooling may result in the lamellar-rod transition.

According to classical solidification theory, a eu-



tectic fibrous structure is much more stable, when the volume fraction of one of the phases is approximately  $0-1/\pi$ . However, Jackson<sup>[19]</sup> and Hunt<sup>[20]</sup> claimed that the change of eutectic structure is correlated with not only the volume fraction of the two phases, but also the anisotropy of eutectic phase itself. When the crystal growth direction is consistent with the solidification rate, the eutectic structure is lamellar eutectic. Otherwise, the eutectic structure is rod one. From Fig.5(a) and Fig.6(a), it can be seen that the crystal growth direction is nearly parallel to the heat flow orientation at the low solidification rate. At the higher crystal growth rate, although the fibers are parallel to each other within the same grain but some fibers are deviated from the original direction at the grain boundaries as shown in Fig.5(b)-6(d). A grain boundary usually consists of structural units which depend on both the misorientation of the two grains and the plane of the interface.

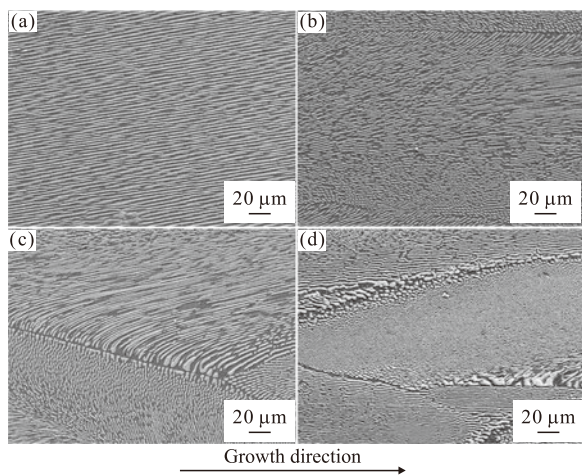


Fig.5 Steady longitudinal microstructures of directionally solidified Fe-Al-Ta eutectic alloy grown at (a)  $R=6\ \mu\text{m/s}$ ; (b)  $R=20\ \mu\text{m/s}$ ; (c)  $R=30\ \mu\text{m/s}$ ; (d)  $R=80\ \mu\text{m/s}$

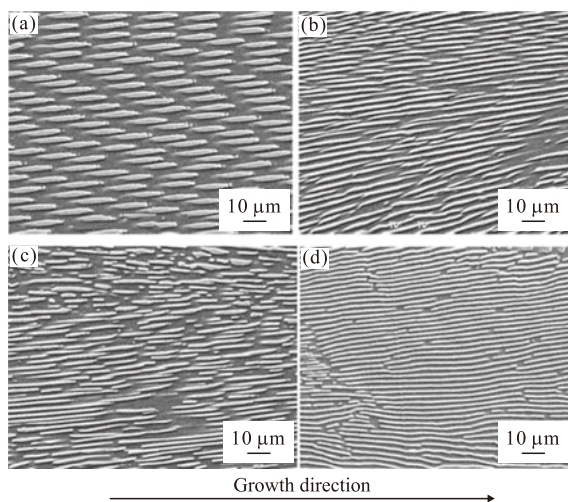


Fig.6 Steady longitudinal microstructures (greater magnification) of directionally solidified Fe-Al-Ta eutectic alloy grown at (a)  $R=6\ \mu\text{m/s}$ ; (b)  $R=20\ \mu\text{m/s}$ ; (c)  $R=30\ \mu\text{m/s}$ ; (d)  $R=80\ \mu\text{m/s}$

Therefore, the higher solidification rate and the anisotropy of the eutectic phase are the factors that result in the lamellar-rod eutectic transition as well.

### 3.3.2 Effect of the solidification rate on the lamella or inter-rod spacing

The lamellar or rod spacing is an important factor to describe the eutectic structure, and it is defined as the distance between the center of one lamellar (or rod) to the center of the nearest adjacent lamellar (or rod). The lamellar or rod spacing of Fe-Al-Ta is obtained by at least 10-30 different regions on the transverse section of the samples. The lamellar or rod spacing of the Fe-Al-Ta eutectic at different solidification rate is shown in Fig.7.

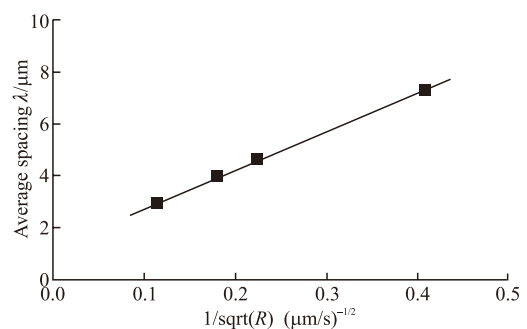


Fig.7 Average spacing ( $\lambda$ ) of Fe-Al-Ta eutectic alloy versus inverse square root of the solidification rate  $R$

For directionally solidified Fe-Al-Ta eutectic alloy, it is a kind of regular eutectic structure; therefore, the lamellar or rod spacing should be in accordance with the Jackson-Hunt criterion<sup>[21]</sup> well as shown in Formula (2):

$$\lambda^2 R = K \tag{2}$$

It can be clearly observed that the lamellar or rod spacing is decreased with the increase of the solidification rate. The constant  $K$  in this work is calculated to be  $1.35 \times 10^5\ \mu\text{m}^3/\text{s}$ .

Moreover, the spacing adjustment is also observed in Fe-Al-Ta eutectic alloy as Fig.8 shows. The new lamellas are formed by branching as arrow A shows; the lamellar is twisted as arrow B shows; the termination of the lamellar is also observed as arrow C shows. In general this several kinds of growth defects can't appear alone. Actually they will appear and develop at the same time to adjust the eutectic lamellar (rod) spacing. The aim of the lamellar spacing adjustment is to accommodate the stress mismatch caused by different growing conditions. According to the minimum undercooling criterion<sup>[22]</sup>, there is an extremum lamellar spacing  $\lambda_e$  which can make the minimum undercooling at a constant growth velocity. Therefore, there are two

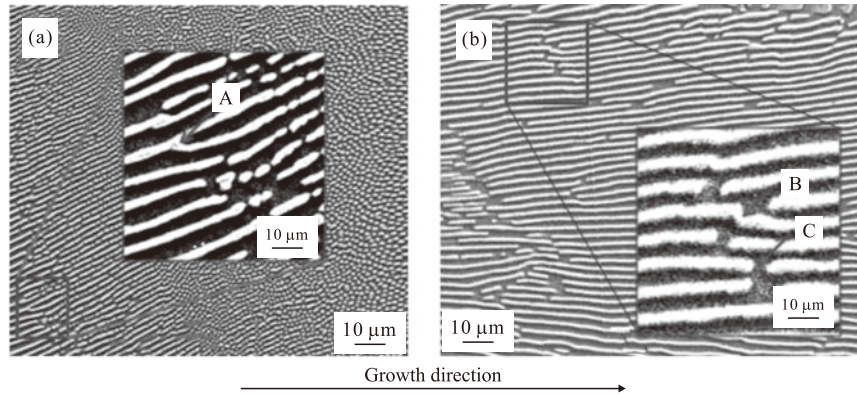


Fig.8 Spacing adjustment observed in Fe-Al-Ta eutectic alloy: (a) branching; (b) twisting and termination

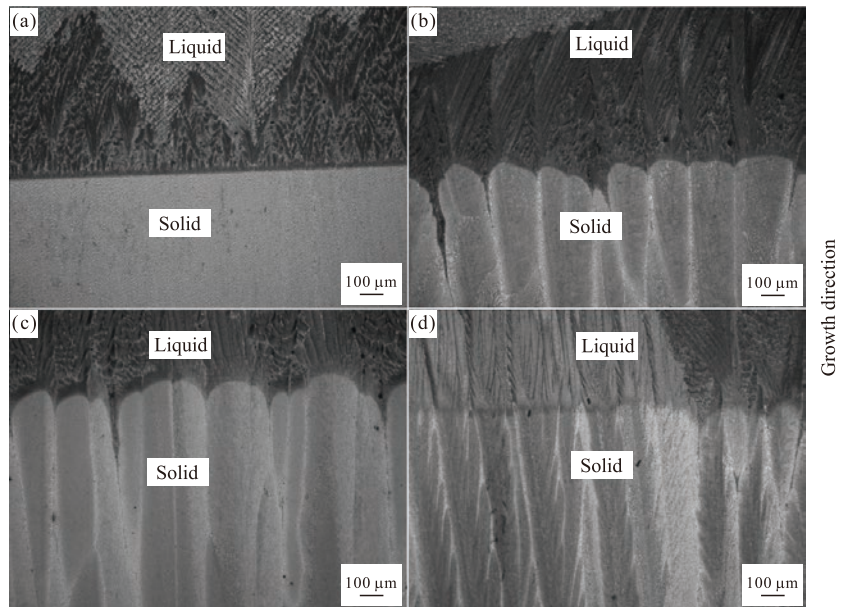


Fig.9 Solid/liquid interface morphologies of directionally solidified Fe-Al-Ta eutectic alloy grown at (a)  $R=6 \mu\text{m/s}$ ; (b)  $R=20 \mu\text{m/s}$ ; (c)  $R=30 \mu\text{m/s}$ ; (d)  $R=80 \mu\text{m/s}$

extreme lamellar spacing on the longitudinal section of the samples, the minimum lamellar spacing  $\lambda_m$  and the maximum lamellar spacing  $\lambda_M$ , respectively. Meanwhile, the average lamellar spacing  $\lambda$  is obtained by measuring on the transverse section of the samples. In general, the lamellar spacing  $\lambda$  for the steady growth at the given solidification rate must obey the condition:

$$\lambda_m < \lambda < \lambda_M \quad (3)$$

when  $\lambda$  is greater than  $\lambda_M$ , tip splitting or branching occurs as arrow A shows, and the lamellar spacing can be decreased. When  $\lambda$  is smaller than  $\lambda_m$ , the lamellar will be twisted or ceased as arrow B and arrow C shows, and the lamellar spacing can be increased.

### 3.4 Effects of solidification rate on morphologies of the solid/liquid interface of the Fe-Al-Ta eutectic alloy

In general, the variation of the lamellar orientation greatly depends on the imposed solidification

conditions and the history-dependent on the initial interface<sup>[23]</sup>. Therefore, it is of importance to study the morphology of the solid/liquid interface. The solid/liquid interface morphologies of the Fe-Al-Ta eutectic at the different solidification rates are shown in Fig.9.

It can be obviously seen from Fig.9 that the solid/liquid interfaces evolves from planar interface to cellular interface, then to shallow cellular interface with the increase of the solidification rate. The solid/liquid interface is stable with a planar morphology at the low solidification rate  $6 \mu\text{m/s}$  as shown in Fig.9(a). When the growth rate increases to  $20 \mu\text{m/s}$ , the interface turns into shallow cellular morphology as described in Fig.9(b). As the growth rate further increases to  $30 \mu\text{m/s}$ , the deep cellular morphology of solid/liquid interface can be observed in Fig.9(c). Generally speaking, the increase of solidification rate can lead to constitutional undercooling in front of solid/liquid interface. Beyond the limit of constitutional undercooling, the planar sol-



id/liquid interface would be destroyed. Moreover, the disturbance within infinitesimal amplitude in front of solid/liquid interface will result in the deformation of the interface. The similar phenomenon was also obtained in Ni-Ni<sub>3</sub>Si eutectic alloy<sup>[24]</sup>. Therefore, at the relatively low solidification rate, the interface evolution complies with the constitutional undercooling law. The solid/liquid interface transforms from planar interface to shallow cellular interface, then to deep cellular with the increase of the solidification rate as shown in Fig.9(a)-9(c). However, the interface tends to be shallow cellular interface at the solidification rate 80 μm/s as shown in Fig.9(d). As far as the Fe-Al-Ta eutectic alloy is concerned, the solute diffusion at the solid/liquid interface becomes strongly localized when the solidification rate further increases and the shallow cellular interface reappears as Kurz described<sup>[25]</sup>. If the undercooling is large enough, an oscillatory instability of the plane front appears, and massive transformation product may therefore take shape with no or partial solute trapping. The boundary layer at the moving interface is so thin that the concentration spike is too small to be visible. Therefore, the solid/liquid interface transforms to shallow cellular interface again.

Solid/liquid interface morphology plays an important role during the solidification processing, which affects the selection and evolution of the solidification microstructure. In the present work, the relationship between microstructure and solid/liquid interface is consistent with classical solidification theory. The morphology of the solid/liquid interface changes from planar interface to cellular interface, and the solidification microstructure changes from Broken-lamellar eutectic to cellular eutectic accordingly.

## 4 Conclusions

a) Microstructure of directionally solidified Fe-Al-Ta eutectic alloy is composed of Fe(Al, Ta) matrix phase and Fe<sub>2</sub>Ta(Al) Laves phase.

b) With the increase of the solidification rate, the eutectic structure transforms from broken-lamellar eutectic to rod-like eutectic. The lamellar or rod spacing is decreased as well. Lamellar adjustments are also observed during directional solidification process.

c) The solid/liquid interface evolves from planar interface to shallow cellular interface, then to deep cellular, and finally to shallow cellular planar with the increase of the solidification rate.

## References

- [1] Cinca N, Lima C R C, Guilemany J M. An Overview of Intermetallics Research and Application: Status of Thermal Spray Coatings[J]. *Journal of Materials Research and Technology*, 2013, 2(1): 75-86
- [2] Zhou R F, Han Y F, Li S H. *High Temperature Structure Materials*[M]. Beijing: National Defence Industry Press, 2006
- [3] Guo J T, Zhou L Z, Yuan C, *et al.* The Microstructure and Mechanical Properties of Several Kinds of Original and Unique High Temperature Alloys[J]. *Transactions of Nonferrous Metals Society of China*, 2011, 21 (2): 237-250
- [4] Hotař A, Kejzlar P, Palm M, *et al.* The Effect of Zr on High-Temperature Oxidation Behaviour of Fe<sub>3</sub>Al-based Alloys[J]. *Corrosion Science*, 2015, 100: 147-157
- [5] Hotař A, Palm M, Kratochvil P, *et al.* High-temperature Oxidation Behaviour of Zr Alloyed Fe<sub>3</sub>Al-type Iron Aluminide[J]. *Corrosion Science*, 2012, 63: 71-81
- [6] Risanti D D, Sauthoff G. Microstructures and Mechanical Properties of Fe-Al-Ta Alloys with Strengthening Laves Phase[J]. *Intermetallics*, 2011, 19: 1 727-1 736
- [7] Farrokhi A, Samadi A, Asadabad M A, *et al.* Characterization of Mechanically Alloyed Nano Structured Fe<sub>3</sub>Al Intermetallic Compound by X-ray Diffractometry[J]. *Advanced Powder Technology*, 2015, 26(3): 797-801
- [8] Janda D, Fietzek H, Galetz M, *et al.* The Effect of Micro-alloying with Zr and Nb on the Oxidation Behavior of Fe<sub>3</sub>Al and FeAl Alloys[J]. *Intermetallics*, 2013,41: 51-57
- [9] Zamanzade M, Vehoff H, Barnoush A. Effect of Chromium on Elastic and Plastic Deformation of Fe<sub>3</sub>Al Intermetallics[J]. *Intermetallics*, 2013, 41: 28-34
- [10] Tapsuan T, Niyomwas S. Effect of Preform Conditions on Synthesis of Fe<sub>3</sub>Al-TiB<sub>2</sub>-Al<sub>2</sub>O<sub>3</sub> Composite by Self-propagating High-temperature Synthesis[J]. *Procedia Engineering*, 2012, 32: 635-641
- [11] Hasemann G, Schneibel J H, George E P. Dependence of the Yield Stress of Fe<sub>3</sub>Al on Heat Treatment[J]. *Intermetallics*, 2012, 21(1): 56-61
- [12] Xiao Z X, Zheng L J, Wang L, *et al.* Microstructure Evolution of Ti-47Al-2Cr-2Nb Alloy in the Liquid-Metal-Cooling (LMC) Directional-solidification Process[J]. *Journal of Wuhan University of Technology-Mater. Sci. Ed.*, 2011, 26(2): 197-201
- [13] Reviere R, Sauthoff G, Johnson D R, *et al.* Microstructure of Directionally Solidified Eutectic Based Fe(Al,Ta)/Fe<sub>2</sub>Ta(Al) Alloys as a Function of Processing Conditions[J]. *Intermetallics*, 1997, 5: 161-172
- [14] Goulart P R, Cruz K S, Spinelli J E, *et al.* Cellular Growth during Transient Directional Solidification of Hypoeutectic Al-Fe Alloys[J]. *Journal of Alloys and Compounds*, 2009, 470: 589-599
- [15] Milenkovic S, Palm M. Microstructure and Mechanical Properties of Directionally Solidified Fe-Al-Nb Eutectic[J]. *Intermetallics*, 2008, 16: 1 212-1 218
- [16] Mota M A, Coelho A A, Bejarano JMZ, *et al.* Fe-Al-Nb Phase Diagram Investigation and Directional Growth of the (Fe,Al)<sub>2</sub>Nb-(Fe,Al,Nb)<sub>ss</sub> Eutectic System[J]. *Journal of Alloys and Compounds*, 2005, 399: 196-201.
- [17] Tiller W A. *Liquid Metals and Solidification*[M]. Cleveland: Amer. Soc. Metal, 1958
- [18] Liu S, Lee J H, Trivedi. Dynamic Effects in the Lamellar-rod Eutectic Transition[J]. *Acta Materialia*, 2011, 59(8): 3 102-3 115
- [19] Jackson K A, Hunt J D. *Lamellar and Rod Eutectic Growth*[M]. New York: Trans. Met. Soc. Aime, 1996
- [20] Hunt J D. The Lamella-rod Transformation in Eutectics[J]. *Journal of the Institute of Metals*, 1966, (94): 2 348-2 351
- [21] Hunt J D, Jackson K A. *Binary Eutectic Solidification*[M]. New York: Transact. Aime, 1966
- [22] Pelcé P, Rochwerger D, Karma A. Oscillatory Instability and Minimum Undercooling Criterion in Directional Solidification[J]. *Journal of Crystal Growth*, 1991, 110(4): 815-822
- [23] Liu G H, Wang Z D, Li X Z, *et al.* Continued Growth Controlling of the Non-preferred Primary Phase for the Parallel Lamellar Structure in Directionally Solidified Ti-50Al-4Nb Alloy[J]. *Journal of Alloys and Compounds*, 2015, 632: 152-160
- [24] Cui C J, Zhang J, Xue T, *et al.* Effect of Solidification Rate on Microstructure and Solid/Liquid Interface Morphology of Ni-11.5 wt%Si Eutectic Alloy[J]. *Journal of Materials Science & Technology*, 2015, 31(3): 280-284
- [25] Jacot A, Sumida M, Kurz W. Solute Trapping-free Massive Transformation at Absolute Stability[J]. *Acta Materialia*, 2011, 59: 1 716-1 724